Overcurvature induced multistability of linked conical frusta: How a 'bendy straw' holds its shape

SCHOLARONE™
Manuscripts

ROYAL SOCIETY OF CHEMISTRY

Soft Matter

ARTICLE TYPE

Overcurvature induced multistability of linked conical frusta: How a 'bendy straw' holds its shape[†]

Nakul P. Bende [a], Tian Yu [b], Nicholas A. Corbin [b], Marcelo A. Dias [d], Christian D. Santangelo [e], James A. Hanna [b,c*] and Ryan C. Hayward [a*]

We study the origins of multiple mechanically stable states exhibited by an elastic shell comprising multiple conical frusta, a geometry common to reconfigurable corrugated structures such as 'bendy straws'. This multistability is characterized by mechanical stability of axially extended and collapsed states, as well as a partially inverted 'bent' state that exhibits stability in any azimuthal direction. To understand the origin of this behavior, we study how geometry and internal stress affect the stability of linked conical frusta. We find that tuning geometrical parameters such as the frustum heights and cone angles can provide axial bistability, whereas stability in the bent state requires a sufficient amount of internal pre-stress, resulting from a mismatch between the natural and geometric curvatures of the shell. We analyze the latter effect through curvature analysis during deformation using X-ray computed tomography (CT), and with a simple mechanical model that captures the qualitative behavior of these highly reconfigurable systems.

Elastic shells that can undergo snap-through transitions between different mechanically stable states provide a powerful means to design shape programmable structures with adaptable form and function [1]. Perhaps the simplest example is a thin hemispherical shell, which can be turned 'inside-out' to yield a locally stable configuration. Numerous studies have aimed to understand the complex geometric and mechanical relationships underlying such behavior, and to thereby enable the design of reconfigurable elastic structures [2–6]. The resulting reconfigurable shells have found applications such as switchable micro-lenses [7], microfluidic pumps [8], and actuators [9–11]. Complementing these engineered examples, many biological mechanisms have been uncovered that exploit snap-through transitions between mechanically stable states of slender elastic structures to achieve rapid motion [12–15].

While much of the literature has focused on *bi*stability, systems that support *multiple* stable states are attractive for the design of highly reconfigurable structures. Interestingly, such multistability can often be found in the simple motif of corrugated cylindrical
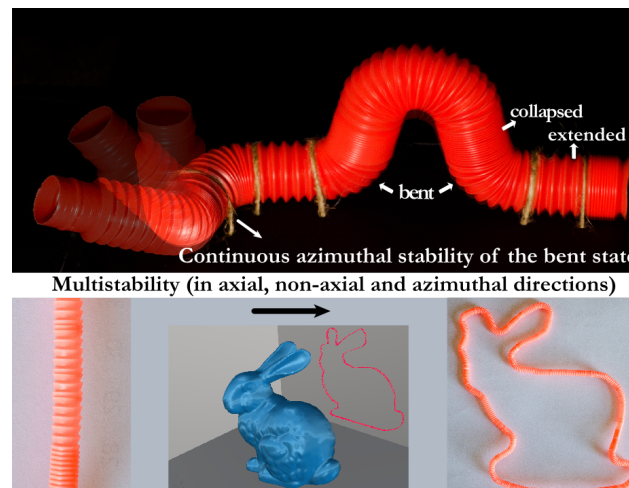
Fig. 1 (Top) Multistability of a *Pop Toob* demonstrated by deforming it into an arbitrary 3D space curve containing extended, collapsed, and bent subunits (overlaid). **(Bottom)** An initially straight section of bendy straw reconfigured into a planar projection of the Stanford bunny model [16].

shells exemplified by a 'bendy straw', and additionally in products such as collapsible bowls, medical tubing, and downspout extenders. This motif consists of repeating units of two non-identical conical frusta in opposing orientations, usually connected at a thinner 'crease'-like region (Fig.1). Multistability in this specific geometry is manifested in the following two ways. Switching between extended and collapsed states through a full inversion of

[a] *Polymer Science and Engineering, University of Massachusetts Amherst, MA, USA*
[b] *Department of Biomedical Engineering and Mechanics, Virginia Polytechnic Institute and State University, Blacksburg, VA, USA*
[c] *Department of Physics & Center for Soft Matter and Biological Physics, Virginia Polytechnic Institute and State University, Blacksburg, VA, USA*
[d] *Department of Engineering, Aarhus University, Aarhus, Denmark*
[e] *Department of Physics, University of Massachusetts Amherst, MA, USA*
∗ Corresponding authors: hayward@umass.edu, hannaj@vt.edu
† Electronic Supplementary Information (ESI) available: SI text, Fig. S1-S7 and Movie M1-M5. See DOI: 10.1039/b000000x/

one frustum, referred to here as 'axial bistability', changes the length of the structure. Additionally, such shells often show stability in a partially inverted (non-axially symmetric) 'bent' state, where the bending direction can be continuously varied while preserving mechanical stability. The versatility of this architecture can be seen in Fig.1, where an arbitrary three-dimensional space curve and a planar projection of the Stanford bunny[16] are formed. Despite the importance of this architecture in a variety of commercial products, the patent literature fails to explore the fundamental mechanisms underlying multistability[17–21].

Axial bistability between extended and collapsed states for each unit of the structure can be understood in much the same manner as for the hemispherical shell described above, and as studied previously in detail for shells with arbitrary curvature[22]. Full inversion of a conical frustum leads to a nearly isometric shape devoid of stretching except at the boundary with the neighboring cone, whereas states intermediate between the two mirror symmetric shapes require stretching of the cone itself. Since the material in the crease is thinner, or otherwise weakened, compared to the rest of the shell, this means that the fully inverted state represents a local minimum in stretching energy, thereby providing mechanical stability as long as the bending energy cost for inversion is not too large (i.e., the shell is sufficiently thin compared to its overall dimensions). However, mechanical stability in the partially inverted state is not as easily understood, yet is vital to the utility of these highly reconfigurable structures.

Geometry and fabrication *

To better understand the behavior of the bendy straw, we simplify the geometry to a single pair of non-identical opposed 'reconfig-

---

* For detailed information on geometry, CAD protocol and molding process, see ESI

urable conical frusta' (RCF) as shown in Fig.2A. The two frusta are defined by the shell thickness (t) and base radius (R), as well as the cone heights (h_1 and h_2) and slant angles (α_1 and α_2) for both the 'upper' and 'lower' frustum. The value of α_1 is larger than α_2 to avoid self-intersection in the collapsed state. One height or angle is constrained by the fact that R is the same between the two frusta. We introduce creased regions (fixed at $t_c = 0.5t$) at the conical bases to guide inversion along this boundary and approximate the thinned portion found in commercial products. We note that the boundary constraints on the two conical bases are important for multistability, and are provided by the neighbouring units in a bendy straw. Here, we impart similar constraints to RCF by connecting the base of each cone to a thick (5 mm) cylindrical shell, which forces these boundaries to remain circular and facilitates gripping during mechanical characterization. We reduce the remaining five-dimensional parameter space for the RCF ($t, R, h_1, \alpha_1, \alpha_2$), by choosing several parameters to match a toy model (*Pop Toob*, Poof-Slinky Inc., USA), i.e., $t/R = 0.017$ (with absolute dimensions increased two-fold to $t = 0.5$ mm) and $\Delta\alpha \equiv \alpha_1 - \alpha_2 = 10^o$, leaving a two-dimensional parameter space spanned by h_1 and α_1. To fabricate elastic RCF, we use a room temperature curable, two-component poly(vinyl siloxane) elastomer (PVS, Elite double 32, Zhermack Inc., Italy; $Y = 1.36$ MPa) for its ease of handling, negligible shrinkage, and consistent material properties. We impart the proper RCF geometry to PVS shells by designing 3D printed, four-part negative molds (Fig.2B), inside which the PVS mixture can be cured (after degassing) to obtain RCF with the desired geometries.

Characterizing RCF stability

We establish the stability of fabricated elastomeric RCF by manipulating them into each shape (extended, collapsed, and bent) by
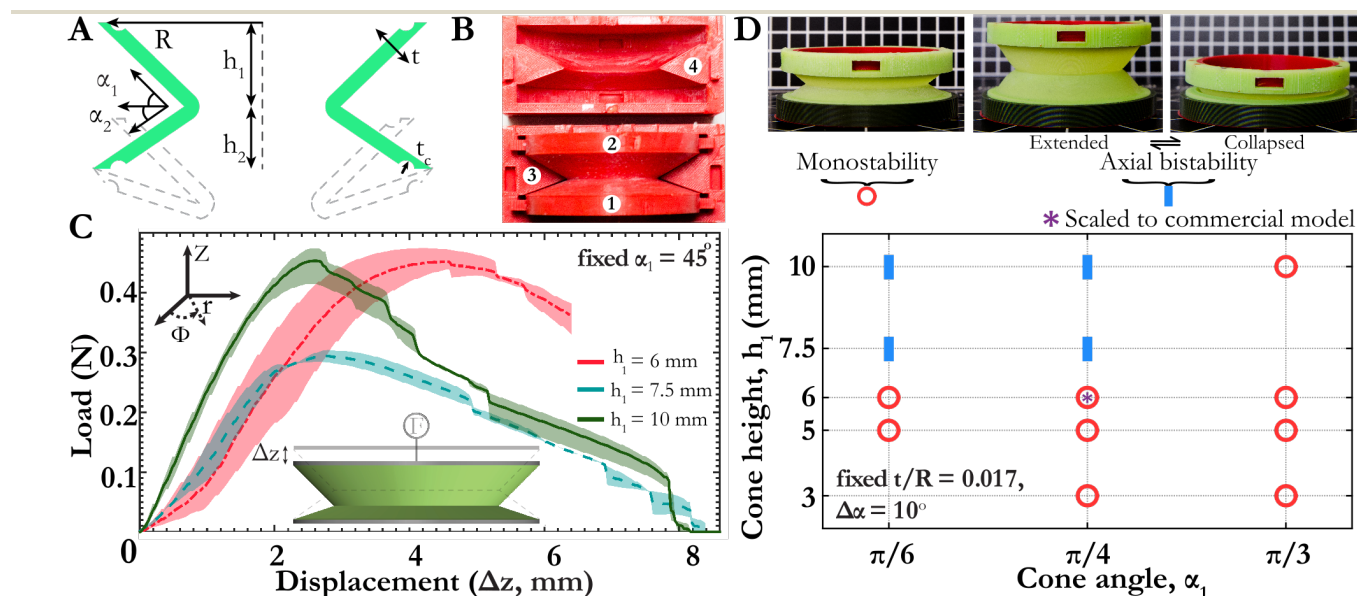

Fig. 2 (A) RCF geometry (collapsed state shown in dashed grey). **(B)** Four-part, 3D-printed negative molds used for curing RCF using poly(vinyl siloxane) elastomer. **(C)** Response under axial load for samples with fixed $\alpha_1 = 45^o$, $\alpha_2 = 35^o$, and varying h_1. Shaded regions show the max/min values around the mean for two runs on three different samples each.**(D)** Stability of elastic RCF with varying h_1 and α_1, recorded for at least 3 samples for each point shown, denoted as monostability ($\bigcirc$), and axial bistability ($\blacksquare$).

hand, with further quantification provided by load/displacement measurements – all carried out with the conical bases rigidly constrained to remain circular using 3D printed grips (see Fig.S3 and S4, ESI). We begin by testing stability for a scaled model of the *Pop Toob* ($h_1 = 6$ mm, $\alpha_1 = 45^o$), which surprisingly shows only monostability (denoted by ◯, Fig.2D). This is further reflected in the axial load-displacement curve (red curve, Fig.2C), which initially shows a monotonic increase in force, followed by a softening when the lower frustum inverts, without the load ever dropping to zero. We also observed monostability for samples with this scaled geometry ($h_1 = 6$ mm, $\alpha_1 = 45^o$) and $\Delta\alpha = 0^o, 5^o$, and 15°, instead of the 10° value used elsewhere in this study. Exploring the parameter space further (with $\Delta\alpha = 10^o$), we observe that setting $h_1 > 6$ mm and $\alpha_1 < 60^o$ results in elastic RCF with axial bistability (denoted by ▌). Here, the response of samples under axial displacement is characterized with force values dropping to zero (around $\Delta z = 8$ mm), indicative of a snap-through transition of the lower frustum to a stable inverted state, resulting in loss of contact between the shell and indenter (Movie M1). The appearance of axial bistability for a sufficiently large cone height is in accordance with the conventional understanding that a sufficiently thin shell is bistable between mirror inversions. However, all of the elastic RCF tested here lack stability in the bent state, failing to capture the multistability that makes the commercial products so useful for shape reconfiguration.

Effect of geometrical frustration on RCF stability
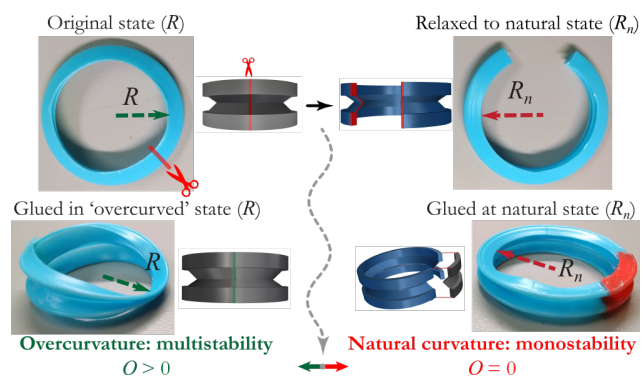
Fig. 3 Effect of overcurvature on multistability of a *Pop Toob*: Cutting a multistable sample opens the structure from an original curvature R to a natural curvature R_n. Gluing the unit back to its original overcurved state restores the multistability (lower left), whereas gluing the unit at the natural radius R_n using an extra piece fails to do so (lower right).

To further investigate the observed lack of stability in the bent state, we reconsider the commercial products that motivate our study. Remarkably, upon cutting axially along one side, the corrugated sections with original base radius R relax by opening up to a natural base radius R_n (Fig.3). This behavior, indicative of a built-in pre-stress, is consistent among several thermoplastic and elastomeric products, including *Pop Toob*, a collapsible dog bowl
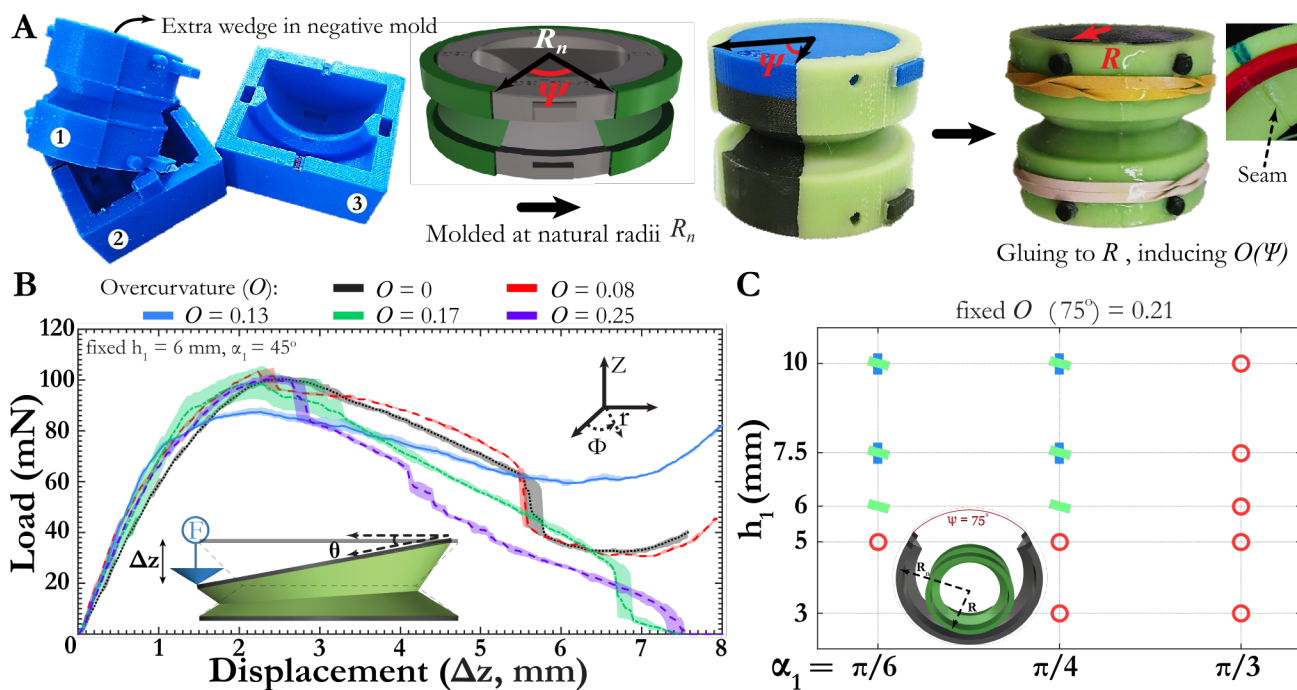
Fig. 4 Introducing overcurvature in RCF : (A) Redesigned three-part molds for fabricating RCF with a wedge of arc angle ψ missing. The molded sample with natural radius R_n is glued by curing uncrosslinked polymer to the intended radius R, introducing a controlled overcurvature $O(\psi)$. **(B)** Response of samples with $h_1 = 6$ mm, $\alpha_1 = 45^o$, $\alpha_2 = 35^o$ and varying O for a non-axial point load. Shaded regions show the max/min values around the mean for two runs each on two different samples. **(C)** A state diagram matching that in Fig. 2C, but now with pre-stress corresponding to $O = 0.21$, demonstrating that stability in the bent state (◥) is induced. Results are recorded for at least three different samples at each point.

(Roysili, USA), and bendy straws. Relieving this pre-stress deprives the structures of stability in both the inverted and bent states, leaving them with a smooth, accordion-like deformation, as shown in Movie M2 for *Pop Toob*. Gluing the structure back to the starting radius R restores multistability. In contrast, closing the sample at its natural radius R_n by gluing in an extra section from another unit restores the topology of the original sample without introducing pre-stress; such samples are also monostable. These observations suggest that sufficient pre-stress, as a result of curvature mismatch, is a necessary condition for stability in the partially inverted bent state, whereas our results on elastic RCF indicate that axial bistability can be achieved for samples of appropriate geometry without pre-stress. The fabrication protocol and material used in this study generate no measurable internal stress due to curing; we observe no dimensional changes after cutting RCF samples open along their axis.

Stress induced by geometrical frustration is known to affect the mechanical equilibria of complex rods[23–25], sheets[26] and shells[27–29]. To explore similar effects of incompatible curvature on the stability of conical frusta, we fabricate elastic RCF with controlled overcurvature by redesigning the negative mold (# 1, Fig. 4A) to include an extra wedge of angle ψ, thus yielding samples with a portion of shell missing. These incomplete shells are molded with natural base radii $R_n(\psi) \equiv R/(1 - \psi/2\pi)$, and then glued closed to radius R by bringing the free edges together and curing additional silicone elastomer applied to the seam. This introduces an internal pre-stress due to the curvature mismatch, or 'overcurvature', quantified as

$$O(\psi) \equiv 1 - \frac{R}{R_n(\psi)} = \frac{\psi}{2\pi}. \quad (1)$$

Introducing pre-stress in this manner slightly increases the dimensions in the axial direction (by $< 10\%$), but offers a simple mechanism for encoding overcurvature in samples with otherwise similar geometry (R, t, t_c, α, h). To study this effect, we program RCF in the previously explored parameter space, but now with $O \equiv$ 0.08 ($\psi = 30^o$), 0.13 (45°), 0.17 (60°), 0.21 (75°) and 0.25 (90°), and measure their stability in the bent state.

A reliable test of stability in the bent state requires a change in tilt angle θ during force-displacement measurements (Fig.4B). We allow for this tilt using linear displacement along the axial (z) direction of an indenter placed at the edge of the shell and allowed to slide freely in the radial (r) direction (see Fig.S4, ESI for CAD schematics and details). Using this non-axial indentation setup, we revisit the scaled *Pop Toob* geometry ($h_1 = 6$ mm, $\alpha_1 = 45^o$), but now with controlled amounts of overcurvature. As shown in Fig.4B, all samples initially show a similar force response: an initial linear regime followed by a peak in force at $\Delta z \approx 2$ mm. Subsequent indentation reveals the effect of overcurvature. Samples with $O = 0.17$ and 0.25 clearly undergo a snap-through transition to a stable bent state, whereas those with lower overcurvature ($O = 0.08$, 0.13) follow a similar force response to the control sample lacking overcurvature (see Movie M3). Following this successful attempt at introducing stability in the bent state for one geometry via pre-stress, we re-investigate the param-

eter space in Fig.2C. We fabricate each geometry in an overcurved state corresponding to $O = 0.21$, and find that all samples with $h_1 \geq 6$ mm and $\alpha_1 < 60^o$ exhibit stability in the bent state upon introduction of overcurvature (denoted by ◥, Fig. 4C). Samples with lower values of h_1, or $\alpha_1 = 60^o$, show no change in stability even at the highest level of overcurvature tested ($O = 0.25$). The partially inverted bent state, whenever stable, is azimuthally degenerate and can be reconfigured in any direction, with the exception of positions near the glued seam where symmetry is broken. Interestingly, samples that initially lacked axial bistability did not gain it through overcurvature, again highlighting that the fundamental requirements for stability in inverted and bent states may be different.

A simple model to capture the effects of geometrical frustration on stability

The creation of new metastable energy minima through frustration is a well known concept, as embodied in canonical examples such as the Ising model on a triangular lattice[30]. To understand how a geometric incompatibility such as overcurvature can lead to multistability, we consider a toy model that captures key qualitative features of RCF . This takes the form of a planar four-bar linkage with two torsional springs (Fig.5A) between a rigid ground link (length $2R$, dashed) and two rigid crank links (length W, shades of red) that prefer rest angles $\tau_l = \alpha_2$ and $\tau_r = (\pi - \alpha_2)$, on the left and right, respectively. Incompatibility is introduced through the disagreement between these rest angles and the length of the rigid floating link ($R - W \cos\beta$, in blue). This seeks to impose a 'cone' angle β different than that of the
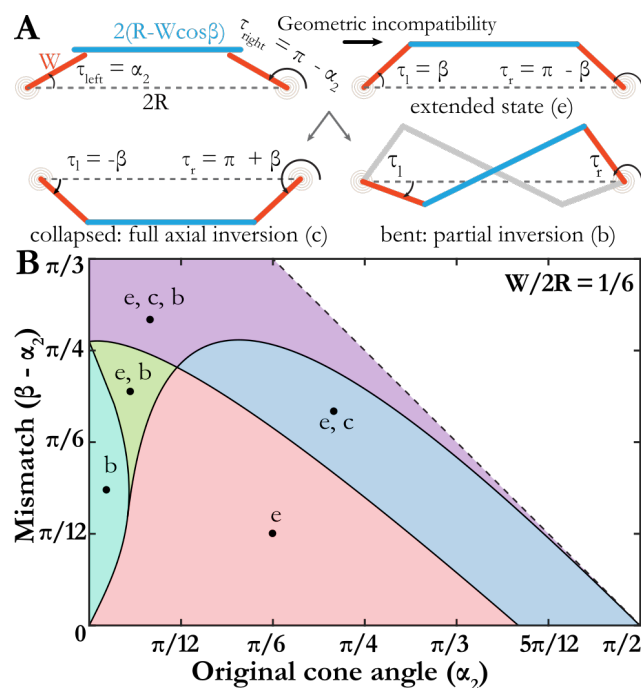
Fig. 5 Incompatible four-bar system: (A) Construction, possible extended, collapsed, and bent states of an incompatible rigid four-bar linkage and torsional spring model. **(B)** Stability of the model for a given link geometry as a function of rest angle and incompatibility.

torsional springs (α_2). Our parameter space is spanned by this mismatch $\beta - \alpha_2$, the original 'cone' angle α_2, and the width W encoded in the length of the crank links. In this minimal model, the interplay between torsional springs, floating link, and ground link is intended to mimic the programmed overcurvature and increase in cone strength arising from the structural surgery, as well as the boundary conditions imposed by neighboring frusta. The possible stable states for this model are the extended state (e) and those obtained from it by full inversion about the ground link to a collapsed (c) state or partial inversion to yield a pair of bent states (e). Four-bar linkages with a single torsional spring were examined by Jensen and Howell, who found conditions for bistability of such structures[31]. A second torsional spring allows for the introduction of frustration or pre-stress, and has also been studied for bistable[32] and tristable[33] four-bar linkages, as pseudo-rigid models of compliant mechanisms.

For our model, we can write the Lagrangian as (complete derivation in ESI),

$$\mathcal{L} = \frac{1}{2}K_r(\tau_l - \alpha_2)^2 + \frac{1}{2}K_r(\pi - \tau_r - \alpha_2)^2 +$$

$$\lambda[(2R + W\cos\tau_r - W\cos\tau_l)^2 + (W\sin\tau_r - W\sin\tau_l)^2$$

$$- (2R - 2W\cos\beta)^2], \tag{2}$$

where K_r is a spring constant and λ a multiplier keeping the crank links at the ends of the floating link. We examine this Lagrangian for incompatibilities $\beta - \alpha_2 > 0$ (analogous to overcurvature) and rest angles $0 \leq \alpha_2 \leq \pi/2$, as shown in Fig.5B. We observe one, two, three, or four stable configurations corresponding to the extended, collapsed, and the pair of bent states.

While the overall behavior is not simple, the general trends are that an increase in geometric incompatibility stabilizes additional states, and that some incompatibility is required to achieve stability in the bent state (b), while stability in the extended (e) or collapsed (c) states can be achieved at zero mismatch. The choice of width W shifts the stability regions, but does not have much of a qualitative effect. The manner in which new states and barriers emerge in the energy landscape is shown in the Fig.S5, ESI. Incompatibility induced stabilization of bent states can be understood by considering a linkage with rest angles α_2 approaching 0, corresponding to a nearly flat cone. Incompatibility in the form of a large floating bar requires deviation from flatness, which is penalized quadratically in the spring energies, approximately $\tau_l^2 + (\pi - \tau_r)^2$ for a nearly-flat cone. Since the magnitudes $|\tau_l|$ and $|\pi - \tau_r|$ are both smaller in the bent state than in either the extended or collapsed states, the bent state becomes the ground state. This region of mechanical stability of the bent state should persist in distorted form as the rest angles increase from zero.

In-situ analysis of deformation pathway for elastic RCF

We return to the 3D shell structures to experimentally characterize their energy landscape by capturing the 3D profile of elastic RCF in situ during deformation using X-ray CT (IVIS SpectrumCT, Perkin Elmer, USA). Tomograms are recorded quasi-statically by

fixing the sample in a deformed state using a custom harness (Fig.S4, ESI), capable of imparting non-axially symmetric deformation in steps of $\Delta z \approx 0.1 - 1$ mm (see Fig.6A). A quantitative analysis of the strain field would require material point tracking at higher resolution than this instrument (with a minimum voxel size of 150 μm) can provide, and marking of a strain grid on these silicone materials risks altering material properties locally. However, curvature analysis on these 3D reconstructions provides Gaussian ($\mathcal{K}$) and mean (H) curvatures in the shells, details of which can be found in the ESI. For thin conical shells, the presence of Gaussian curvature can be taken as a qualitative proxy for stretching, a costlier deformation pathway compared to bending.
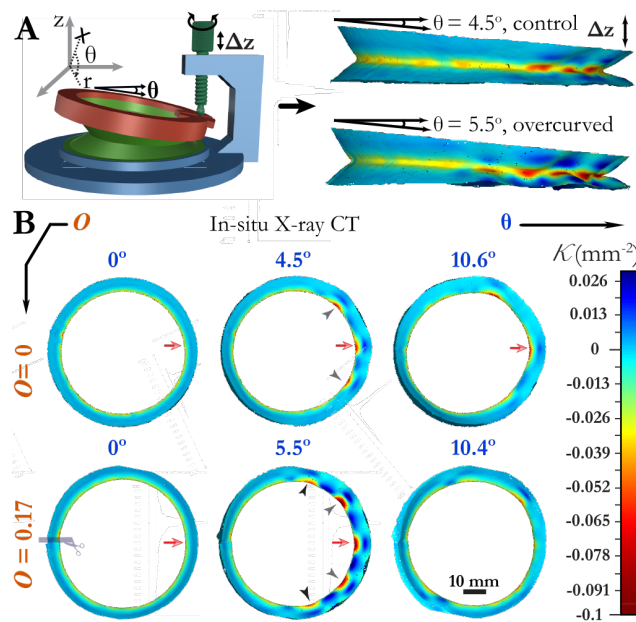
Fig. 6 Non-axial deformation of RCF in natural overcurved states: **(A)** Schematics of the 3D printed harness for in situ X-ray CT studies. Side views of control ($O = 0$) and overcurved ($O = 0.17$) RCF shells at similar levels of tilt angle θ are also shown, with $\mathcal{K}$ projected. **(B)** $\mathcal{K}$ during non-axial loading for control [top row] and overcurved [bottom row] shells, as viewed from the top. Both shells possess similar geometrical parameters ($h_1 = 6$ mm, $\alpha_1 = 45^o$), yet a higher magnitude of $\mathcal{K}$ is seen for the overcurved sample in the intermediate state.

To compare non-axial deformation with and without overcurvature, we plot $\mathcal{K}$ projected onto the surface of RCF ($h_1 = 6$ mm, $\alpha_1 = 45^o$) fabricated with $O = 0$ and $O = 0.17$. In Fig.6B, we compare tomograms in undeformed ($\theta = 0^o$), intermediate ($\theta \approx 5^o$), and bent ($\theta \approx 10^o$) states. As expected in the undeformed state, we observe $\mathcal{K} = 0$ in the conical regions and $\mathcal{K} < 0$ in the highly curved region where the cones attach to each other (see Fig.2A). Upon indentation to $\theta \approx 5^o$, buckled regions with a higher concentration of $\mathcal{K}$ ('crests' marked with black and gray arrows) are seen near the point of indentation (red arrow). Throughout the deformation pathway, overcurvature leads to an increase in both the number of discernible crests and an increase in the magnitude of $\mathcal{K}$ associated with each crest (see side views). Indenting the sample further to $\theta \approx 10^o$ brings both of the RCF to the partially inverted configuration, though only the overcurved sample is stable in this bent state. The higher

number of crests in the overcurved sample remains consistent throughout the entire non-axial indentation, supporting the idea that overcurvature increases the energetic cost of intermediate states enough to create an energy barrier that allows for stability in the partially inverted bent state.

Additive manufacturing of plastic RCF

Finally, we present a simple protocol for fabrication of overcurved RCF out of viscoelastic polymers. Notably, the residual stress in an overcurved *Pop Toob* is lost when it is left in an extended state for more than $\approx$ 1-2 days (see Movie M4). Conversely, one can imagine harnessing viscoelastic behavior to induce overcurvature. As a proof-of-concept, we directly 3D print tiled RCF using a commercially available poly(urethane) based filament (Cheetah, NinjaTek, USA, using an Ultimaker 2 Extended+, Ultimaker, the Netherlands), as shown in Fig.7.

The as-printed RCF ($h_1 = 10$ mm, $\alpha_1 = 45^o$) lack any overcurvature and are monostable. A controlled amount of overcurvature, and resulting multistability, in these samples can be introduced by constraining them into a collapsed state for a fixed duration (Fig.7C, Movie M5). The minimum time needed to induce sufficient overcurvature for multistability can be empirically found by measuring the opening angle after cutting the sample open along the axis (Fig. S7, ESI). Indeed, the time-scale over which this pre-stress develops ($\tau \approx 3.2$ h) corresponds closely to the measured time of 3 h after which the samples achieve stability in the bent state. Leaving a sample in an uncompressed state for extended times is sufficient to reverse the process of imparting overcurvature. While further exploration is necessary, this initial result suggests that the use of viscoelastic relaxation to impart desired pre-stresses in shells may lead to more direct and rapid fabrication of more complex multistable structures from a wider range of materials.
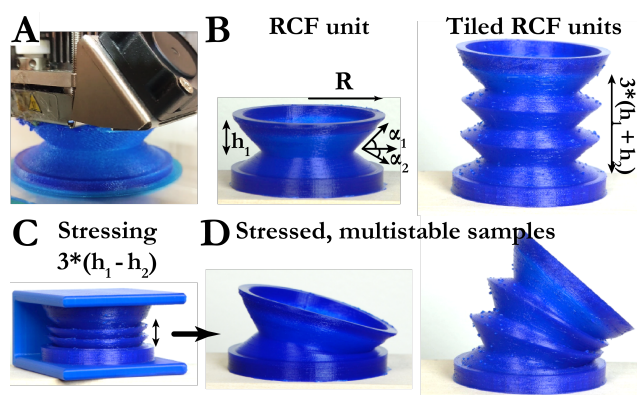
Fig. 7 3D printed RCF : (A) 3D printing of an RCF using a poly(urethane) based elastomer. **(B)** Printed single-RCF and tri-RCF . **(C)** Fixing the elastomer shell under a collapsed state for $\approx$ 3 hours introduces a built-in residual stress for NinjaTek Cheetah. **(D)** RCF with built-in stress demonstrating stability in the bent state.

Conclusions

Structures with a high degree of geometric reconfigurability have recently garnered interest for use in surgical tools[34], deployable mechanisms[35] and robotic arms[36]. As a modular structure, the

bendy straw offers an attractive architecture in such contexts, although the mechanism by which it supports multiple mechanically stable states has remained unknown until now. In this report, we explored the multistability of linked conical shells using experiments and a mechanical model, and established protocols for fabricating reconfigurable conical frusta with controlled overcurvature (pre-stress) in elastic and viscoelastic materials. We have established that axial stability between extended and collapsed states can be achieved through careful selection of geometrical parameters (cone height h_1, slant angle α_1 and thickness t), while stability in bent, partially inverted, states requires a combination of appropriate geometry and sufficient pre-stress, at least over the range of parameter space studied. A simplified four-bar linkage model provides qualitative insight into how geometric frustration can stabilize both collapsed and bent states. For the full three-dimensional shell geometry, an analysis of the spatial distributions of curvatures during deformation indicates that the effect of overcurvature is to increase the stretching energy in the intermediate state during non-axial deformation, thereby providing an energy barrier and rendering the bent state metastable. We suspect that overcurvature in commercial products made with thermoplastic polymers may be a result of stresses induced by the forming process or long term storage in a collapsed state.

References

1 N. Hu and R. Burgueño, *Smart Materials and Structures*, 2015, **24**, 063001.
2 C. R. Calladine, *Theory of shell structures*, Cambridge University Press, 1989.
3 A. Pippard, *European Journal of Physics*, 1990, **11**, 359.
4 K. Seffen, *Scripta materialia*, 2006, **55**, 411–414.
5 A. Pandey, D. E. Moulton, D. Vella and D. P. Holmes, *Europhys. Lett.*, 2014, **105**, 24001.
6 A. Reid, F. Lechenault, S. Rica and M. Adda-Bedia, *Physical Review E*, 2017, **95**, 013002.
7 D. Holmes and A. Crosby, *Adv. Mater.*, 2007, **19**, 3589–3593.
8 B. Tavakol, M. Bozlar, C. Punckt, G. Froehlicher, H. A. Stone, I. A. Aksay and D. P. Holmes, *Soft Matter*, 2014, **10**, 4789–4794.
9 M. R. Shankar, M. L. Smith, V. P. Tondiglia, K. M. Lee, M. E. McConney, D. H. Wang, L.-S. Tan and T. J. White, *Proc. Natl. Acad. Sci. U.S.A.*, 2013, **110**, 18792–18797.
10 V. Ramachandran, M. D. Bartlett, J. Wissman and C. Majidi, *Extreme Mechanics Letters*, 2016, **9**, 282–290.
11 S. A. Zirbel, K. A. Tolman, B. P. Trease and L. L. Howell, *PloS one*, 2016, **11**, e0168218.

12 Y. Forterre, J. M. Skotheim, J. Dumais and L. Mahadevan, *Nature*, 2005, **433**, 421–425.

13 M. Hayashi, K. L. Feilich and D. J. Ellerby, *Journal of Experimental Botany*, 2009, **60**, 2045–2053.

14 M. Smith, G. Yanega and A. Ruina, *J. Theor. Biol.*, 2011, **282**, 41–51.

15 K. Son, J. S. Guasto and R. Stocker, *Nature Physics*, 2013, **9**, 494–498.

16 G. Turk and M. Levoy, Proceedings of the 21st annual conference on Computer graphics and interactive techniques, 1994, pp. 311–318.

17 J. B. Friedman, *Flexible drinking straw*, 1951, US Patent 2,550,797.

18 H. J. Harp, W. T. Leible and W. M. Mccort, *Flexible drinking tube*, 1968, US Patent 3,409,224.

19 E. Mikol, *Adjustable tubular wall structure for connectors and the like*, 1989, US Patent 4,846,510.

20 E. J. Diebolt and R. A. Hendrickson, *Tubular hinge assembly*, 1975, US Patent 3,929,165.

21 D. Kusuma, P. M. Card and H. J. B. Lugo, *Collapsible container*, 2010, US Patent 7,654,402.

22 N. P. Bende, A. A. Evans, S. Innes-Gold, L. A. Marin, I. Cohen, R. C. Hayward and C. D. Santangelo, *Proceedings of the National Academy of Sciences*, 2015, **112**, 11175–11180.

23 P.-O. Mouthuy, M. Coulombier, T. Pardoen, J.-P. Raskin and A. M. Jonas, *Nature communications*, 2012, **3**, 1290.

24 M. A. Dias and B. Audoly, *Journal of Elasticity*, 2015, **119**, 49–66.

25 B. Audoly and K. A. Seffen, *Journal of Elasticity*, 2015, **119**, 293–320.

26 E. Efrati, E. Sharon and R. Kupferman, *J. Mech. Phys. Sol.*, 2009, **57**, 762–775.

27 E. Kebadze, S. Guest and S. Pellegrino, *International Journal of Solids and Structures*, 2004, **41**, 2801–2820.

28 K. A. Seffen and S. D. Guest, *Journal of Applied Mechanics*, 2011, **78**, 011002.

29 W. Hamouche, C. Maurini, A. Vincenti and S. Vidoli, *Meccanica*, 2016, **51**, 2305–2320.

30 R. Moessner and A. P. Ramirez, *Phys. Today*, 2006, **59**, 24.

31 B. D. Jensen and L. L. Howell, *Journal of Mechanical Design*, 2003, **125**, 701–708.

32 B. Jensen, L. Howell and L. Salmon, *Journal of Mechanical Design*, 1999, **121**, 416–423.

33 T. M. Pendleton and B. D. Jensen, *Journal of Mechanical Design*, 2008, **130**, 122302.

34 M. Cianchetti, T. Ranzani, G. Gerboni, I. De Falco, C. Laschi and A. Menciassi, Intelligent Robots and Systems (IROS), 2013 IEEE/RSJ International Conference on, 2013, pp. 3576–3581.

35 E. T. Filipov, G. Paulino and T. Tachi, *Proc. R. Soc. A*, 2016, **472**, 20150607.

36 S. Kamrava, D. Mousanezhad, S. M. Felton and A. Vaziri, *Advanced Materials Technologies*, 2018, **3**, 1700276.